ELSEVIER

Catalysis Today 42 (1998) 167–174

CATALYSIS TODAY

Catalytic activity of perovskite-type oxide catalysts for direct decomposition of NO: Correlation between cluster model calculations and temperature-programmed desorption experiments

Yasuharu Yokoi*, Hiroshi Uchida

Fundamental Technology Research Laboratory, Tokyo Gas Co., Ltd., 16-25, 1-chome, Shibaura, Minato-ku, Tokyo 105, Japan

Abstract

The relationship between NO decomposition activity on lanthanum transition metal oxide catalysts (transition metal=Cr, Mn, Fe, Co and Ni) and their oxygen desorption properties was investigated by using catalytic activity measurements, temperature-programmed desorption (TPD), X-ray photoelectron spectroscopy (XPS) and molecular orbital calculations. The NO decomposition activity correlated with both the amount of O_2 desorbed and the temperature of O_2 desorption. The variations in the temperature of O_2 desorption during TPD could be explained by electronic interaction with the transition metal. The variations in the O1s photoline observed by XPS could be explained by the variations in the charge of the surface oxygen species, which was affected by the electronic interaction with the transition metal. Molecular orbital techniques are powerful tools in NO decomposition catalyst research.

Keywords: NO decomposition; Perovskite-type oxide catalyst; Temperature-programmed desorption; Molecular orbital calculation; X-ray photoelectron spectroscopy

1. Introduction

Nitrogen oxides (NO_x) are formed during various combustion processes. They are pollutants that contribute to acid rain, cause the formation of ozone in the troposphere by photochemical oxidation, and they affect the respiratory system of humans and animals. It is therefore important to reduce these emissions as much as possible [1].

Nitrogen monoxide (NO) is thermodynamically unstable relative to N_2 and O_2 at temperatures below 1000°C, and therefore its catalytic decomposition ($2NO \rightarrow N_2+O_2$) is the simplest and cheapest method to remove NO from exhaust streams [2].

In the development of NO decomposition catalysts, the promotion of oxygen desorption from the catalyst surface remains the main subject of concern despite the fact that more serious problems need to be overcome with practical catalysts. Oxygen from dissociated NO is often strongly bonded to the catalyst surface, poisoning NO dissociation site and preventing further NO dissociation. Therefore, to promote oxygen desorption from the catalysts at a lower temperature is one effective approach for improving NO decomposition catalysts. Although extensive catalyst searching and screening studies have continued, there

*Corresponding author. Tel.: +81-3-5484-4817; fax: 81-3-3453-7583; e-mail: yyokoi@tokyo-gas.co.jp

0920-5861/98/$32.00
PII S0920-5861(98)00087-X

is no sufficient practical catalyst to decompose NO that is highly active and durable [3]. Some innovative solution to the design of NO decomposition catalysts would be indispensable in breaking through this deadlock. We believe that a clarification of the correlation between oxygen desorption properties and the electronic structure of the catalyst surface will enable us to obtain important information on NO decomposition catalyst design [4–6].

In the present study, we investigated the relationship between NO decomposition catalysis and oxygen desorption properties which we evaluated by temperature-programmed desorption (TPD) experiments. TPD is known as an effective method to investigate reactivity on the catalyst surface, which is greatly affected by its electronic state. While, X-ray photoelectron spectroscopy (XPS) measurement is widely used to characterize the catalyst surface, especially its electronic state. Therefore, we investigated the relationship between the TPD profile and XP spectra. Furthermore, we attempted to interpret the results from both TPD experiments and XPS measurements through model calculation using molecular orbital methods.

The catalysts focused on in the present work were lanthanum transition metal oxides with the chemical composition $LaMO_3$ (M: transition metal=Cr, Mn, Fe, Co and Ni) and having perovskite-type structures [7]. The $LaMO_3$ system is suitable to study the relationship between NO decomposition activity and oxygen desorption properties, which may be affected by the electronic interaction between the transition metal and oxygen.

2. Experimental

2.1. Preparation and characterization of catalysts

The $LaMO_3$ (M=Cr, Mn, Fe, Co, Ni) catalysts were prepared by calcining precursor powder synthesized by spray pyrolysis (Praxair Specialty Ceramics) at 650°C for 1 h and at 850°C for 5 h in air. To measure catalytic activity, we pressed the calcined powder into pellets, then crushed, and sieved them to 40–80 mesh size.

Powder X-ray diffraction analysis was carried out with a Phillips PW3020 diffractometer operating at 40 kV and 40 mA, which used Cu K_α radiation combined with a nickel filter.

The BET specific surface area of the catalysts was determined via nitrogen adsorption at −196°C after the catalyst was degassed at 300°C for 3 h in a high vacuum.

The X-ray photoelectron spectra were recorded with a Kratos XSAM 800 ESCA system. Mg K_α radiation (1253 eV) was used as the source and the base pressure in the analyzer chamber was maintained at less than 10^{-8} Torr. Instrument control as well as data collection and processing were done using Kratos Vision software. The resulting binding energy values were corrected by the C1s peak at 284.6 eV. The O1s spectrum was deconvoluted with the Gaussian method and an auto-fit built-in program was used.

2.2. Catalytic activity measurement

Catalytic activity measurements were carried out using a fixed-bed flow system with a quartz tubular reactor (10 mm i.d.) under atmospheric pressure. The procedure used to evaluate the catalytic activity of all catalysts was as follows: first, 5 g of catalyst was charged into the reactor; next, a flow of He was passed through the reactor at 100 cm^3/min and the temperature was raised to 600°C at a rate of 10°C/min. Catalytic reaction was then started. A gas mixture of NO (1 vol%) and He (balance) was fed at a flow rate of 100 cm^3/min (W/F=3.0 g s cm^{-3}). The reaction temperature was increased stepwise from 600°C to 700°C. All experimental data were taken after 3–4 h on stream at each temperature while the catalytic reaction completely reached a steady state. The reactor effluent was analyzed by gas chromatography using a molecular sieve 5A column for N_2 and O_2 and a Porapak Q column for N_2O. The catalytic activity for NO decomposition was evaluated in terms of the conversion of NO to N_2 ($2[N_2]$out/[NO]in) and that of NO to O_2 ($2[O_2]$out/[NO]in).

2.3. TPD experiments

TPD following O_2 adsorption (TPD of O_2) was carried out in a flow quartz reactor tube (6 mm i.d.). The catalyst (weight 0.25 g) held on quartz wool was pretreated under an O_2 flow (20 cm^3/min) at 800°C for 1 h and then cooled to room temperature.

Then a He flow was substituted for the O_2 flow. After this, the system was purged with He (50 cm^3/min) until no change in the O_2 concentration could be detected. The catalyst was heated to 800°C at a constant heating rate of 20°C/min, using ultra high purity helium as the carrier gas, at a flow rate of 50 cm^3/min. O_2 desorbed during the heating was detected by an on-line mass spectrometer.

TPD following NO adsorption (TPD of NO) was carried out in the same flow quartz reactor tube as that used for the TPD of oxygen. The 0.25 g catalyst was pretreated under a He flow (20 cm^3/min) at 700°C for 1 h and then cooled to room temperature. NO adsorption was then carried out by flowing a mixture of NO (1 vol%)/He (balance) at 20 cm^3/min through the sample bed at ambient temperature for 30 min. After this, the system was purged with He (50 cm^3/min) until no change in the NO concentration could be detected. The catalyst was heated to 800°C at a constant heating rate of 20°C/min, using ultra high purity helium as the carrier gas, at a flow rate of 50 cm^3/min. The effluent was monitored by mass spectrometer for the following species: m+/e: 28 for N_2, 30 for NO, 32 for O_2, 44 for N_2O and 46 for NO_2.

2.4. Molecular orbital calculations

To investigate the electronic interaction between the oxygen and the transition metal on the $LaMO_3$ surface, the molecular orbitals of the cluster (M_2O_8+O_2) and cluster (M_2O_8+O) were calculated using the DV-Xα cluster method [8]. The former was a model for the adsorbed O_2, the latter was a model for the lattice oxygen, on the $LaMO_3$ surface. The clusters were assumed to have the structure in Fig. 1. The bond order for M–O(1) in the cluster (M_2O_8+O_2) calculated by overlap population analysis was evaluated as the value corresponding to the force preventing O_2 desorption in order to compare with the temperature of O_2 desorption from the $LaMO_3$ during the TPD experiments. The charges of the O(1), O(2) and O(3) were evaluated in order to compare with the electronic state of the surface oxygen species observed by XPS.

The details on the calculations are as follows. The distance between M and O was assumed to be the experimental value for each $LaMO_3$ (about 0.19 nm) and an ideal cubic structure was assumed for all

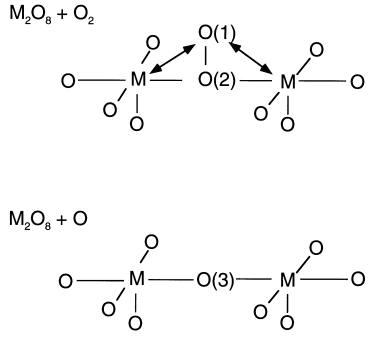

Fig. 1. Structure of clusters. M_2O_8+O_2: adsorbed O_2 on the $LaMO_3$ surface; M_2O_8+O: surface lattice oxygen on the $LaMO_3$ surface.

$LaMO_3$ unit cells. The bond length for O(1)–O(2) was assumed to be 0.12 nm. We assumed that the total charge of the cluster (M_2O_8+O) was determined by the sum of the formal charge of the component ions (M=+3, O=−2) and 1, which was added as the compensating charge due to the polarity of the $LaMO_3$ (100) surface [9]. The total charge of the cluster (M_2O_8+O_2) was assumed to be the value determined by balancing the Fermi level of the cluster (M_2O_8+O). We use embedded cluster models in which point charges are located at the lattice points in the perovskite structure and on the cluster surface. This takes into account the effect of the Madelung electrostatic potentials of the ions surrounding the clusters. We assumed the conventional values for the point charges, that is +3, +3 and −2 for La, M and O ions, respectively.

3. Results

3.1. Characterization

X-ray diffraction showed that all catalysts prepared in this study had perovskite-type structures as reported in the previous literature [7,10]. The specific surface areas of the catalysts (in m^2/g) were as follows: $LaCrO_3$, 5.7; $LaMnO_3$, 2.7; $LaFeO_3$, 4.1; $LaCoO_3$, 2.0; $LaNiO_3$, 4.3.

The X-ray photoelectron spectra of the catalysts in the O1s region are shown in Fig. 2. The spectra were similar to those previously reported [11]. They had two peaks. One was a sharp peak located

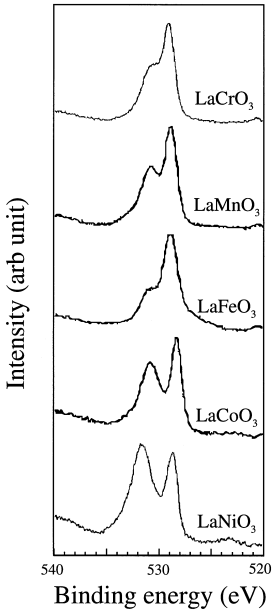

Fig. 2. X-ray photoelectron spectra of $LaMO_3$ (M=Cr, Mn, Fe, Co, Ni) in the O1s region.

at 528.3–528.9 eV (O_L peak). The other was a broad peak located at the higher binding energy region (O_H peak). Generally, the former was assigned to lattice oxygen and the latter was assigned to adsorbed oxygen [11]. The O1s photolines were deconvoluted to the O_L and the O_H. The binding energy value, the full width half maximum (FWHM) of each peak and the peak intensity ratio O_H/O_L are listed in Table 1. The FWHM of the O_L peak for $LaFeO_3$ was so large that the O1s photoline of $LaFeO_3$ could not be deconvoluted to the two species.

Table 2
NO decomposition activity of the catalysts

Catalyst	NO conversion to N_2 (%)		NO conversion to O_2 (%)	
	600°C	700°C	600°C	700°C
$LaCrO_3$	0.0	0.3 (0.05)	0.0	0.0
$LaMnO_3$	1.3	3.6 (1.33)	0.6	0.7
$LaFeO_3$	0.6	0.8 (0.20)	0.0	0.0
$LaCoO_3$	4.3	5.7 (2.85)	0.7	1.0
$LaNiO_3$	13.1	23.7 (5.51)	3.3	8.5

Values in parentheses are NO conversions to N_2 per specific surface area (% g m^{-2}).

3.2. NO *decomposition activity*

Table 2 shows the conversion of NO to N_2 and O_2. Little formation of N_2O was observed for all the catalysts tested at both 600°C and 700°C. The conversions of NO to N_2 were not equal to that of NO to O_2. This suggested that NO_2 was produced by the reaction $NO+1/2O_2 \rightarrow NO_2$ in the reactor lines and the chromatographic column during analysis [12]. Therefore, the conversion of NO to N_2 was regarded as the net activity.

3.3. *TPD of* O_2

The O_2 desorption profiles from $LaMO_3$ during the TPD of O_2 are shown in Fig. 3. The temperatures from 40°C to 600°C are defined as 'the lower temperature range' and the temperatures from 600°C to 800°C are defined as 'the higher temperature range' in the present paper. The profiles except for $LaFeO_3$ exhibited a

Table 1
Deconvoluted data for the X-ray photoelectron spectra of the catalysts in the O1s region

Catalyst	First peak (O_L)		Second Peak (O_H)		Peak intensity ratio (O_H/O_L)
	BE[a] (eV)	FWHM[b] (eV)	BE (eV)	FWHM (eV)	
$LaCrO_3$	528.93	1.23	530.56	2.81	0.60
$LaMnO_3$	528.81	1.19	530.71	3.01	0.62
$LaFeO_3$[c]	—	—	—	—	—
$LaCoO_3$	528.30	1.16	530.78	2.70	0.74
$LaNiO_3$	528.63	1.27	531.52	2.92	1.07

[a]Binding energy.
[b]Full width half maximum.
[c]Impossible to deconvolute into O_L and O_H because of broadening (see text).

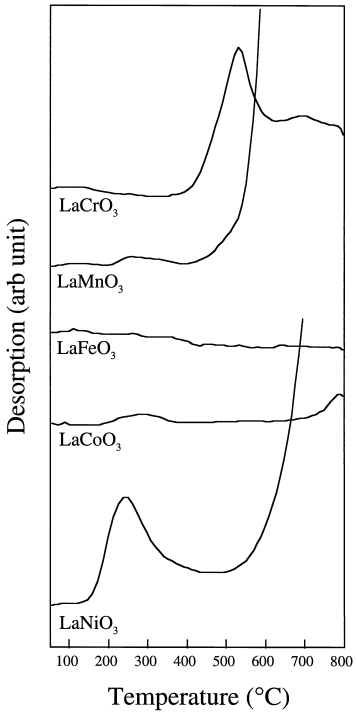

Fig. 3. O_2 desorption profiles from $LaMO_3$ (M=Cr, Mn, Fe, Co, Ni) during TPD of O_2.

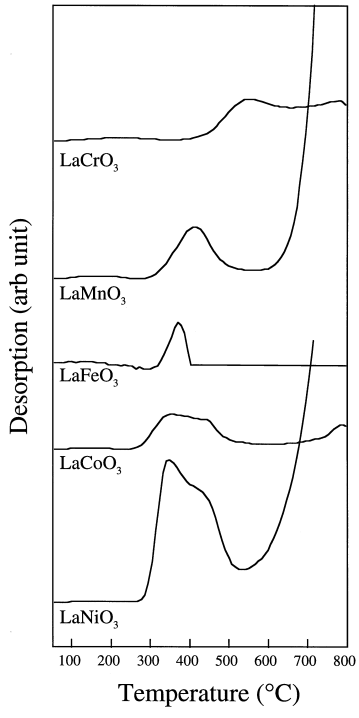

Fig. 4. O_2 desorption profiles from $LaMO_3$ (M=Cr, Mn, Fe, Co, Ni) during TPD of NO.

peak in the higher temperature range, which was assigned as O_2 desorption from the lattice oxygen in bulk by Teraoka et al. [13]. They had already reported similar profiles to those in Fig. 3 except for $LaCrO_3$ [13].

On the other hand, the O_2 desorption in the lower temperature range was as follows: The profile for $LaCrO_3$ exhibited a desorption peak at 529°C overlapping the peak at 695°C, while Teraoka et al. reported that there was no oxygen desorption below 800°C [13]. For $LaMnO_3$, at temperatures above 203°C, adsorbed oxygen began to be desorbed and it exhibited a peak at 257°C. Similar results have already been reported by Nitadori et al. [14]. There was no desorption peak for $LaFeO_3$, although Nitadori et al. reported the existence of one [15]. For $LaCoO_3$, the O_2 began to be desorbed at 181°C and exhibited a peak at 284°C. Similar results have also already been reported by Nakamura et al. [16]. For $LaNiO_3$, the desorption began at 138°C and exhibited a peak at 234°C, which was similar to that recently reported by Zhao et al. [17].

3.4. *TPD of* NO

The O_2 desorption profiles from $LaMO_3$ during the TPD of NO are shown in Fig. 4. In the higher temperature range, the profiles almost equal those during the TPD of O_2. On the other hand, in the lower temperature range, the profiles are more distinguishable and larger than those during the TPD of O_2 except for $LaCrO_3$. Especially for $LaFeO_3$, there is a distinct desorption peak at 370°C in spite of the absence of O_2 desorption during the TPD of O_2.

The NO desorption profiles during the TPD of NO are shown in Fig. 5. The NO desorption profiles at the highest desorption temperature (300–600°C) are identical with the O_2 desorption profiles at corresponding temperatures in Fig. 4 except for $LaCrO_3$. Quantitative analysis revealed that the ratio of the O_2 desorbed to the NO desorbed at this peak is about unity for $LaMnO_3$, $LaFeO_3$, $LaCoO_3$ and $LaNiO_3$. During the NO adsorption before TPD and during TPD itself, very little N_2, N_2O and NO_2 were detected.

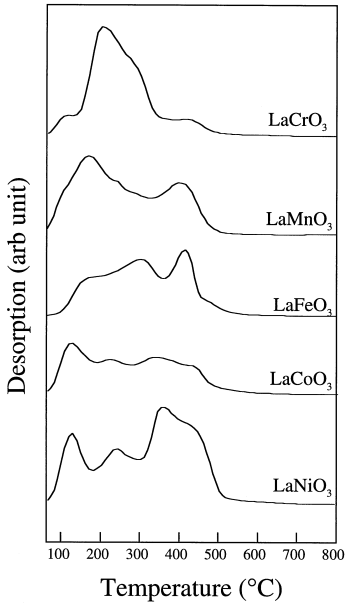

Fig. 5. NO desorption profiles from $LaMO_3$ (M=Cr, Mn, Fe, Co, Ni) during TPD of NO.

3.5. Molecular orbital calculations

Convergent results were obtained by spin-unrestricted calculations except in the case of M for Ni. Spin-restricted calculations were carried out for Ni and these converged.

The bond order for M–O(1) was calculated as shown in Table 3. The bond order decreased with the increasing atomic number of the transition metal. This indicated that the strength of the force preventing O_2 desorption decreased with the increasing atomic number of the transition metal.

The charges of O(1), O(2) and O(3) were calculated as shown in Fig. 6. The calculated charge of the adsorbed O_2 (namely O(1) plus O(2)) was negative. This indicated that electron transfer occurred from the catalyst to adsorbed O_2 in comparison with a free O_2 molecule. The extent of the charge transfer decreased with the increasing atomic number of the transition metal. The charge of the adsorbed O_2 became more positive with the increasing atomic number of the transition metal. On the other hand, the charge of the surface lattice oxygen O(3) was more negative than O(1) or O(2). The charge of surface lattice oxygen also tended to be more positive with the increasing atomic number of the transition metal.

Table 3
Bond order of M–O(1) shown in Fig. 1

$LaMO_3$	Bond order for M–O(1) (e)
$LaCrO_3$	0.216
$LaMnO_3$	0.182
$LaFeO_3$	0.112
$LaCoO_3$	0.112
$LaNiO_3$	0.110

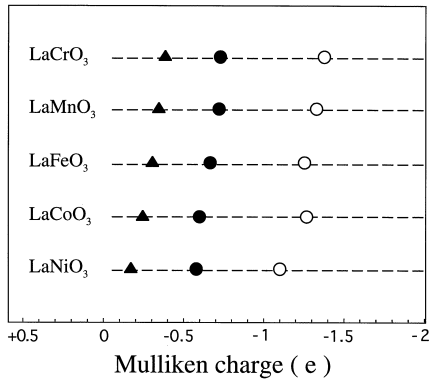

Fig. 6. The calculated charges of various oxygen species in Fig. 1: (▲) O(1); (●) O(2); (○) O(3).

4. Discussion

4.1. Amount of O_2 desorbed during TPD

The catalysts had the higher NO decomposition activity, when the amount of O_2 desorbed during TPD increased. The catalytic activity measurements revealed that the $LaNiO_3$ had the highest NO decomposition activity of the catalysts tested. $LaCoO_3$ as well as $LaMnO_3$ had the second highest activity and $LaCrO_3$ and $LaFeO_3$ had a little activity. The order of the amount of O_2 desorption in the lower temperature range during the TPD of O_2 was as follows: $LaNiO_3$>-$LaCrO_3$>$LaMnO_3$=$LaCoO_3$≫$LaFeO_3$ which paralleled the NO decomposition activity except for $LaCrO_3$, which desorbed O_2 at a relatively higher temperature. The desorption of lattice oxygen in bulk

was not clearly correlated with the NO decomposition activity in the present study, although Teraoka et al. [18] and Zhao et al. [17] had reported this correlation.

The amount of O_2 desorption at the lower temperature range during the TPD of NO also correlated with NO decomposition activity. It should be noted that the O_2 desorption in $LaCrO_3$ was relatively smaller than that during the TPD of O_2. The order for the amount agreed with the order for NO decomposition activity. Further, the O_2 desorption in $LaFeO_3$ was detected during the TPD of NO, while no oxygen desorption could be detected during the TPD of O_2. Since very little N_2, N_2O and NO_2 were detected as mentioned in Section 3.4, the O_2 desorbed during the TPD of NO might not be produced by NO dissociation.

The oxygen species O_H observed by XPS is generally assigned as adsorbed oxygen, which is weakly bounded on the perovskite-type oxide surface [13]. Thus, an appropriate amount of desorbed O_2 in proportion to the O_H peak intensity of each catalyst is expected. However, the amount of O_2 desorbed during the TPD of O_2 did not completely correlate with the O_H peak intensity. In particular, there was a distinguishable O_H peak in the O1s photoline of $LaFeO_3$, while no O_2 desorption occurred during the TPD of O_2. On the other hand, the amount of O_2 desorbed during the TPD of NO correlated well with the O_H peak intensity. These findings suggested that the O_2 desorbed during the TPD of NO might be correlated with the O_H species.

4.2. *Temperature of* O_2 *desorption during TPD*

Generally, the temperature of O_2 desorption should be correlated with NO decomposition catalysis, since it should be related to the activation energy for O_2 desorption. Therefore, with lower O_2 desorption temperatures from the catalyst, the NO decomposition activity is expected to be higher. In the present study, the order for the NO decomposition activity in Table 2 agreed with the order for the temperature of O_2 desorption in the lower temperature range during the TPD of O_2 except for $LaFeO_3$, which desorbed no O_2 during the TPD of O_2.

The temperature of O_2 desorption during the TPD of O_2 tended to decrease with the increasing atomic number of the transition metal. We estimated the strength of the force preventing O_2 desorption by model calculations using the molecular orbital methods as a result of speculating that the temperature of O_2 desorption was affected by the electronic interaction between the adsorbed O_2 and the transition metal. The calculated bond order for M–O(1) listed in Table 3 became smaller with the increasing atomic number of the transition metal. Therefore, the variations in the bond order could explain the variations in the temperature of O_2 desorption during the TPD of O_2. This strongly suggested that the temperature of O_2 desorption from the lanthanum metal oxide during the TPD of O_2 was affected by the electronic interaction between the adsorbed O_2 and the transition metal.

As for the TPD of NO as well as the TPD of O_2, the temperature of O_2 desorption decreased with the increasing atomic number of the transition metal. However, the temperature of O_2 desorption tended to become higher than that during the TPD of O_2. This indicated that the O_2 desorption mechanism in the TPD of NO differed from that in the TPD of O_2. As the O_2 desorption accompanied the NO desorption, the O_2 desorption in the TPD of NO was considered to be too complicated to be dealt with in the same manner as the O_2 desorption in the TPD of O_2.

4.3. *Explanation of variations in* O1s *photoline*

It has been reported that the binding energy of the O_H peak of $LaMO_3$ (M=Cr, Mn, Fe, Co and Ni) is shifted higher with the increasing atomic number of the transition metal [11]. We obtained similar results in the present study. We estimated the charge of the O_2 or O on the $LaMO_3$ by model calculations using molecular orbital methods as shown in Fig. 6, since we speculated that binding energy shifting was caused by variations in the charge of the surface oxygen species. The calculated charge of both O_2 and O shown in Fig. 6 tended to become more positive with the increasing atomic number of the transition metal. Therefore, the variations in the calculated charge could explain binding energy shifting. This strongly suggested that the binding energy shifting of the O_H peak was caused by the difference in the electronic interaction between the transition metal and the O_H species, which probably consisted of several oxygen species such as adsorbed O_2, surface lattice oxygen, and so on.

The peak intensity ratio O_H/O_L listed in Table 1 tended to increase with increasing atomic number of the transition metal, although the disorder was observed for $LaFeO_3$. This was similar to the previous results [11]. According to molecular orbital theory, a free molecule has two unoccupied $2\pi^*$ antibonding orbitals. Consideration that the charge transfer from the catalyst to the adsorbed O_2 decreased with the increasing atomic number of the transition metal as Fig. 6 shows, the stability of the adsorbed O_2 should be more stable with the increasing atomic number of the transition metal. Therefore, the increase in the O_H peak intensity with the increasing atomic number of the transition metal was reasonable according to our calculated results.

5. Conclusions

1. The NO decomposition activity in the lanthanum transition metal oxide catalysts correlated with their oxygen desorption properties such as the amount of O_2 desorbed and the temperature of O_2 desorbed from the catalysts.
2. The variations in the temperature of O_2 desorption could be explained by electronic interaction with the transition metal.
3. The variations in the O1s photoline could also be explained by the variations in the charge of the surface oxygen species, which was affected by electronic interaction with the transition metal.
4. Molecular orbital techniques are powerful tools in NO decomposition catalyst research. In future, we will apply them to more serious problems such as the poisoning of coexisting gases: O_2, H_2O, SO_2, CO_2 and so on.

Acknowledgements

This study has been performed as a part of the national project 'Development of Ceramic Gas Engine' coordinated by The Japan Gas Association, which administered the project with the financial support of the Japanese government (Ministry of International Trade and Industry, MITI).

References

[1] J.N. Armor, Appl. Catal. B 1 (1992) 221.
[2] J.W. Hightower, D.A Van Leirsberg, in: R.L. Klimish, J.G. Larsonv (Eds.), The Catalytic Chemistry of Nitroge Oxides, Plenum Press, New York, 1975, p. 63.
[3] M. Iwamoto, H. Yahiro, Catal. Today 22 (1994) 5.
[4] Y. Yokoi, I. Takahashi, H. Uchida, Hyomen Kagaku 16 (1995) 448.
[5] Y. Yokoi, H. Uchida, in: Proceedings of the 11th International Congress on Catalysis, Baltimore, 1996.
[6] Y. Yokomichi, T. Nakayama, O. Okada, Y. Yokoi, I. Takahashi, H. Uchida, H. Ishikawa, R. Yamaguchi, H. Matsui, T. Yamabe, Catal. Today 29 (1996) 155.
[7] E.J. Baran, Catal. Today 8 (1990) 133.
[8] M. Tsukada, C. Satoko, H. Adachi, J. Phys. Soc. Jpn. 48 (1980) 200.
[9] M. Tsukada, N. Shima, Phys. Chem. Minerals 15 (1987) 35.
[10] J. Wang, H. Yasuda, K. Inumaru, M. Misono, Bull. Chem. Soc. Jpn. 68 (1995) 1226.
[11] J.L.G. Fierro, L.G. Tejuca, Appl. Surf. Sci. 27 (1987) 453.
[12] Y. Li, W.K. Hall, J. Phys. Chem. 94 (1990) 6145.
[13] Y. Teraoka, M. Yoshimatsu, N. Yamazoe, T. Seiyama, Chem. Lett. (1984) 893.
[14] T. Nitadori, S. Kurihara, M. Misono, J. Catal. 98 (1986) 221.
[15] T. Nitadori, M. Misono, J. Catal. 93 (1985) 459.
[16] T. Nakamura, M. Misono, Y. Yoneda, Bull. Chem. Soc. Jpn. 55 (1982) 394.
[17] Z. Zhao, X. Yang, Y. Wu, Appl. Catal. B 8 (1996) 281.
[18] Y. Teraoka, H. Fukuda, S. Kagawa, Chem. Lett. (1990) 1.